*Wear*, 42 (1977) 9 - 22



# VARIATIONAL METHOD FOR FINITE LENGTH SQUEEZE FILM DAMPER DYNAMICS WITH APPLICATIONS

P. E. ALLAIRE, L. E. BARRETT and E. J. GUNTER

*Department of Mechanical Engineering, University of Virginia, Charlottesville, Va. 22901 (U.S.A.)*

(Received May 28, 1976)

## Summary

A variational method of solving Reynolds' equation and of determining the load capacity analytically is obtained for the finite length squeeze film damper undergoing full dynamic motion. The method is then used to determine effective damper coefficients for circular synchronous precession and a non-linear transient analysis is carried out for several damper configurations.

---

## 1. Introduction

Squeeze film dampers have been investigated in a number of recent works as devices to reduce unbalance response or increase stability [1 - 7]. In some cases critical speeds or stability threshold speeds can be moved out of the operating range of rotating machinery. Analysis and experience have shown that damper characteristics must be carefully chosen for a particular machine, or use of the damper may actually make problem vibrations worse [5, 7].

The initial design of dampers often involves sizing of the damper using effective stiffness and damping coefficients followed by non-linear transient analysis [7]. Effective coefficients are obtained by assuming that the damper undergoes circular synchronous precession, which is often approximated in real dampers. Non-linear transient analysis is then carried out to verify the linear approach. The final step must be to evaluate the complete rotor–bearing system including the damper.

Analytical solutions to Reynolds' equation are preferable to numerical solutions where they are available. This is particularly true for non-linear transient analysis where the cost of a numerical method may be prohibitive. Most analytical solutions of squeeze film dampers employ the short bearing approximation [1 - 7]. It is accurate for small length-to-diameter ratios at small to moderate operating eccentricities but can give substantial errors for high eccentricities or high squeeze rates. Another approximation is that of

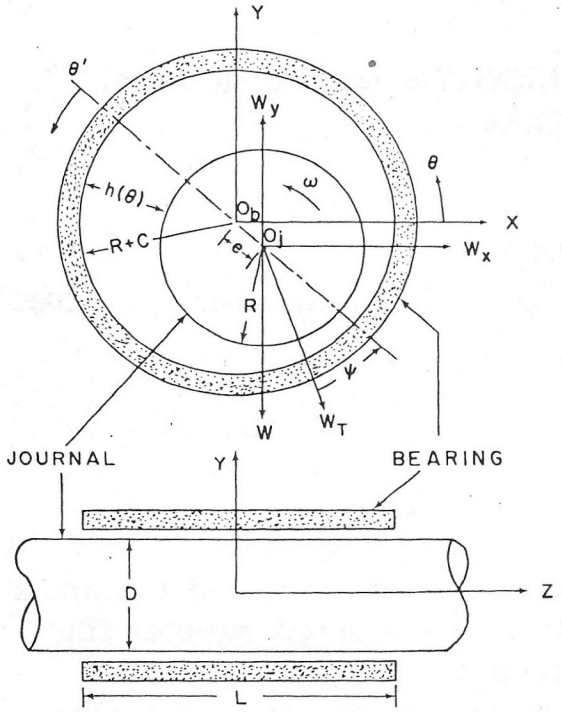


Fig. 1. Schematic of squeeze film damper.

the long bearing, which is appropriate if the damper is completely sealed at the ends and has no circumferential oil supply groove [4]. An alternative approach without approximation is the variational method applied by Hays [8] to a 180° journal bearing subjected to vertical sinusoidal loads.

This work extends the initial work of Hays [8, 9] to the variational analysis of 360° finite length dampers. A doubly infinite trigonometric series solution for the pressure has been obtained for completely general dynamic damper motion. The solution has been applied to stiffness and damping characteristics for circular synchronous precession and to non-linear transient motions.

## 2. Equations of motion

Figure 1 shows a schematic of a squeeze film damper. Reynolds' equation is

$$\frac{\partial}{\partial \alpha}\left(\frac{\bar{h}^3}{12\pi S}\frac{\partial \bar{P}}{\partial \alpha}\right)+\frac{1}{4\bar{L}^2}\frac{\partial}{\partial \bar{z}}\left(\frac{\bar{h}^3}{12\pi S}\frac{\partial \bar{P}}{\partial \bar{z}}\right)=2\frac{\partial \bar{h}}{\partial t} \tag{1}$$

where

$$\bar{h}=1+\bar{e}\cos\alpha \qquad \alpha=\theta-\theta_{\max} \tag{2}$$

The variational principle $\bar{J}(\bar{P})$ to be minimized is

$$\bar{J}(\bar{P}) = \int_0^1 \int_0^{2\pi} \left[ \frac{\bar{h}^3}{24\pi S} \left\{ \left( \frac{\partial \bar{P}}{\partial \alpha} \right)^2 + \frac{1}{4\bar{L}^2} \left( \frac{\partial \bar{P}}{\partial \bar{z}} \right)^2 \right\} + 2 \frac{\partial \bar{h}}{\partial \bar{t}} \bar{P} \right] d\alpha \, d\bar{z} \tag{3}$$

The boundary conditions for the damper are that the pressure is periodic in the circumferential direction and that it vanishes at the edges:

$$\bar{P}|_{\alpha} = \bar{P}|_{\alpha+2\pi} \tag{4}$$

$$\left. \frac{\partial \bar{P}}{\partial \alpha} \right|_{\alpha} = \left. \frac{\partial \bar{P}}{\partial \alpha} \right|_{\alpha+2\pi} \tag{5}$$

$$\bar{P}|_{\bar{z}=0} = 0 \tag{6}$$

$$\bar{P}|_{\bar{z}=1} = 0 \tag{7}$$

Ambient pressure is neglected.

These boundary conditions are appropriate for a number of damper configurations other than the one with open ends shown in Fig. 1. Many dampers have a circumferential oil groove at the center, making the pressure zero at $\bar{z} = \frac{1}{2}$, and end seals restricting end leakage to negligible amounts. The resulting pressure profile is identical to that for the uniform damper with open ends. Also, if there is no circumferential oil groove but the approximate flow rate and pressure drop across the seal can be calculated, the pressure just inside the seal can be added as a constant to the pressure calculated from eqns. (3) - (7).

A trigonometric series solution of the form

$$\bar{P}(\alpha, \bar{z}) = \sum_{l=1}^{\infty} \left[ \sum_{k=1}^{\infty} \{A_{kl} \sin k\alpha + B_{kl} \cos (k-1)\alpha\} \right] \sin l\pi\bar{z} \tag{8}$$

is assumed. Each term satisfies eqns. (4) - (7). The variational principle is minimized if the equations

$$\frac{\partial \bar{J}}{\partial A_{kl}} = 0 \qquad \frac{\partial \bar{J}}{\partial B_{kl}} = 0 \tag{9}$$

are satisfied by the constants $A_{kl}$ and $B_{kl}$. These two sets of equations result in uncoupled equations for the constants, as shown in the Appendix.

The radial and tangential dimensionless forces are obtained by integration as

$$\bar{F}_r = \frac{1}{2} \int_0^1 \int_{\alpha_c}^{\alpha_c+\pi} \bar{P} \cos\alpha \, d\alpha \, d\bar{z} \tag{10}$$

$$\bar{F}_t = \frac{1}{2} \int_0^1 \int_{\alpha_c}^{\alpha_c+\pi} \bar{P} \sin\alpha \, d\alpha \, d\bar{z} \tag{11}$$

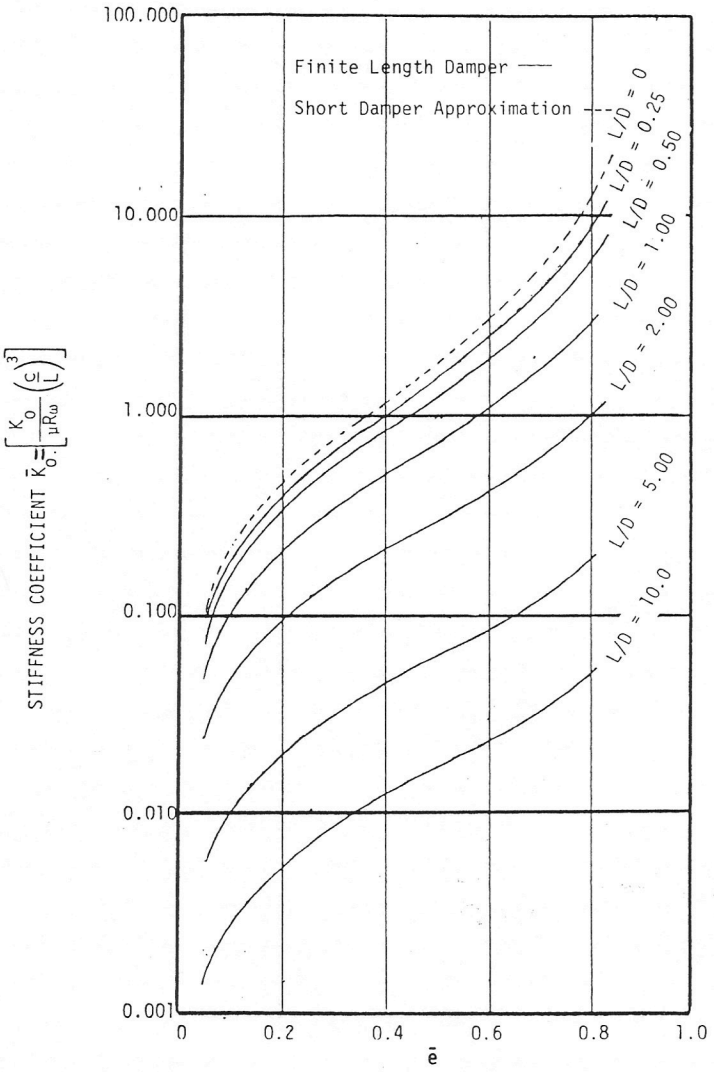


Fig. 2. Stiffness coefficient *vs.* eccentricity for the finite length damper and short damper approximations.

where $\alpha_c$ is the angle at which the positive pressure regions begins. This angle is given by

$$\alpha_c = \tan^{-1}\left(\frac{\partial \bar{e}}{\partial \bar{t}} \Big/ -\bar{e}\frac{\partial \phi}{\partial \bar{t}}\right) \tag{12}$$

Detailed results are shown in the Appendix. If ambient pressurization is to be included, the extent of the positive pressure region must be determined numerically and eqns. (10) and (11) modified accordingly.

## 3. Stiffness and damping coefficients

Effective stiffness and damping coefficients for the damper may be obtained by assuming that the damper undergoes circular synchronous precession about the damper center. For this case

$$\frac{\partial \phi}{\quad} \qquad \frac{\partial \bar{e}}{\quad} \qquad 0$$

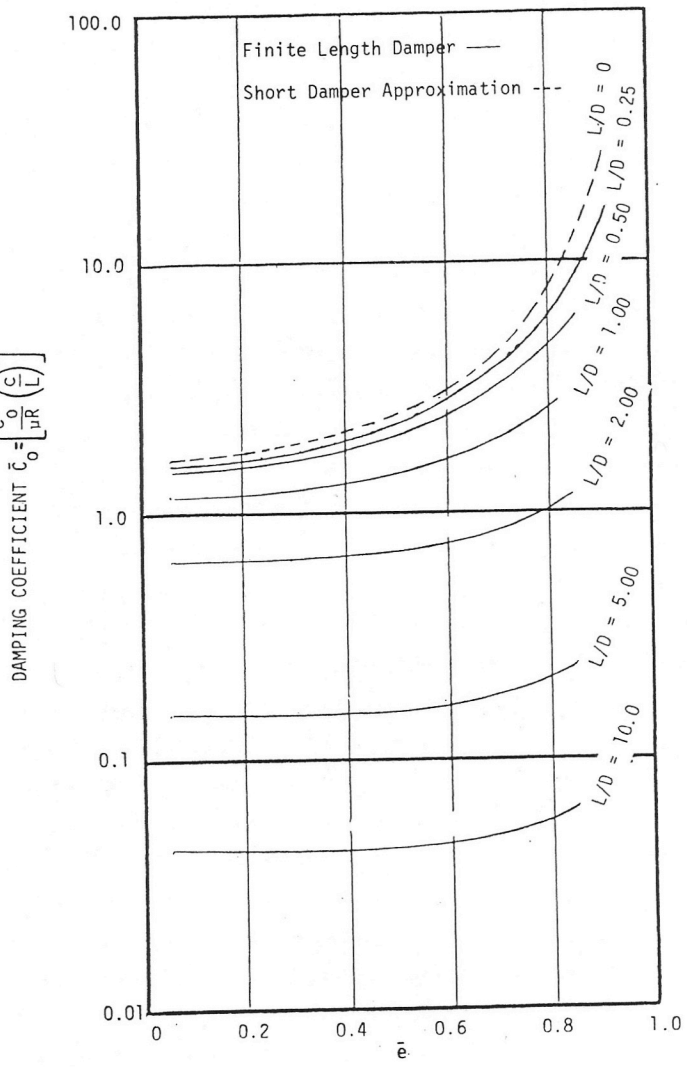


Fig. 3. Damping coefficient *vs.* eccentricity for the finite length damper and short damper approximations.

and all of the $B_{kl}$ terms have zero value. Equations (A3) and (A4) reduce to

$$\bar{F}_r = \frac{2}{\pi} \sum_{\substack{l=1 \\ \text{odd}}}^{\infty} \frac{1}{l} \left( \sum_{k=1}^{\infty} A_{2k,l} \frac{2k}{4k^2 - 1} \right) \tag{13}$$

$$\bar{F}_t = \frac{1}{2} \sum_{\substack{l=1 \\ \text{odd}}}^{\infty} \frac{1}{l} A_{1,l} \tag{14}$$

The effective stiffness and damping coefficients are obtained from ref. 7 as

$$\bar{K}_0 = -\frac{Wc^2 \bar{F}_r}{\mu R \omega L^3 \bar{e}} \tag{15}$$

and

$$= \frac{Wc^2 \bar{F}_t}{}$$

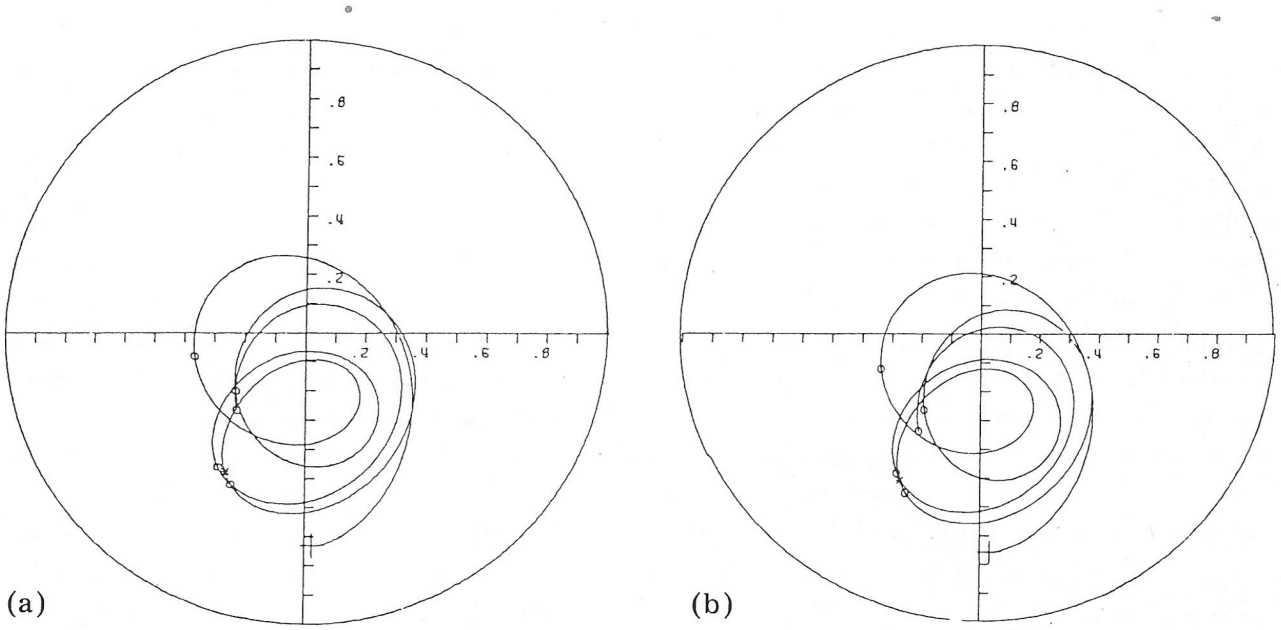


Fig. 4. Transient response of a damper with $L/D = 2/7$ and $\bar{e}_u = 0.25$. (a) Short bearing approximation for a horizontal squeeze film bearing with a cavitated film. The parameters are: W 675.0 lb; L 2.000 in; C 7.00 mil; PS 0.00 lb $in^{-2}$; WX 0.00 lb; FU 3699.90 lb; KRX 50 000 lb $in^{-1}$; TRD 1.05; N 10 500 rev $min^{-1}$; R 3.500 in; MU 2.490 microreyn; FMAX 3877.4 lb; WY 0.00 lb; KRY 50 000 lb $in^{-1}$. (b) Finite length theory for a horizontal finite squeeze film bearing with a cavitated film. The parameters are as in (a) except: TRD 1.02; FMAX 3768.4 lb.

The rotating parameter $\omega$ used for making the parameters dimensionless is the precession rate $\partial\phi/\partial t$.

Figures 2 and 3 show the stiffness and damping characteristics for a damper employing the short bearing approximation ($L/D = 0$) [1] and for finite length dampers. For small $L/D$ ratios the short and finite damper results are in good agreement, except at large eccentricities where they begin to diverge. As the $L/D$ ratio begins to increase, the dimensionless coefficients fall off rapidly in magnitude although the curves retain the same general shape as the eccentricity increases. The stiffness increases rapidly with increasing eccentricity while the damping remains relatively constant.

The stiffness and damping characteristics shown in Figs. 2 and 3 give good preliminary clearance design data for a squeeze film damper. For example, typical values for stabilizing a ten-stage compressor subject to aerodynamic cross coupling were found to be $K_0 < 3.50 \times 10^7$ N $m^{-1}$ (200 000 lb $in^{-1}$) and $C_0 \approx 52\,500$ N s $m^{-1}$ (300 lb s $in^{-1}$) [11]. A damper with the properties $R = 8.89$ cm (3.5 in), $L = 17.78$ cm (7.0 in), $W = 3002$ N (675 lb), $\mu = 0.017$ Pa s ($2.49 \times 10^{-6}$ lb s $in^{-2}$) and $\omega = 1099$ rad $s^{-1}$ must have a clearance of $c \approx 0.058$ cm (0.023 in) to achieve the proper values. The actual damper stiffness is $2.36 \times 10^7$ N $m^{-1}$ (135 000 lb $in^{-1}$) but a retainer spring of stiffness $8.76 \times 10^6$ N $m^{-1}$ (50 000 lb $in^{-1}$) is required to center the damper. This damper will be used for the transient analysis shown in

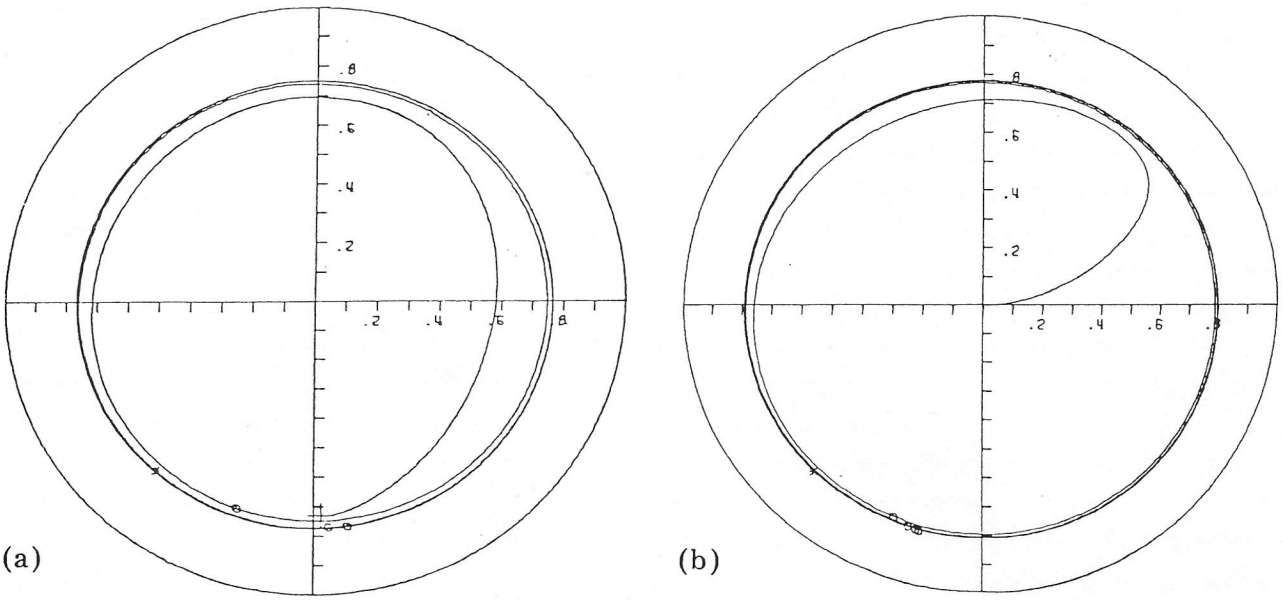


Fig. 5. Transient response of a damper with $L/D$ = 2/7 and $\bar{e}_u$ = 0.50. (a) Short bearing approximation for a horizontal squeeze film bearing with a cavitated film. The parameters are as in Fig. 4(a) except: FU 7399.81 lb; TRD 2.15; FMAX 15 891.4 lb. (b) Finite length theory for a horizontal finite squeeze film bearing with a cavitated film. The parameters are as in (a) except: TRD 1.83; FMAX 13 505.9 lb.

## 4. Non-linear transient response

The non-linear transient equations of motion for a fixed $x$-$y$ coordinate system are, in dimensionless form,

$$\frac{d^2\bar{x}}{d\bar{t}^2} = \bar{F}_x\left(\bar{x}, \bar{y}, \frac{d\bar{x}}{d\bar{t}}, \frac{d\bar{y}}{d\bar{t}}\right) + \bar{e}_u \cos \bar{t} \tag{17}$$

$$\frac{d^2\bar{y}}{d\bar{t}^2} = -\bar{W} + \bar{F}_y\left(\bar{x}, \bar{y}, \frac{d\bar{x}}{d\bar{t}}, \frac{d\bar{y}}{d\bar{t}}\right) + \bar{e}_u \sin \bar{t} \tag{18}$$

Both the hydrodynamic forces $\bar{F}_x$ and $\bar{F}_y$ are functions of journal position and velocity. They are determined at each time step by taking vector components of $\bar{F}_r$ and $\bar{F}_t$ as the equations of motion are integrated forward in time.

A comparison of non-linear transient motion for the short bearing approximation and the finite length analytical solution is shown in Figs. 4(a) and 4(b) respectively. In both cases $L/D$ = 2/7 and the starting conditions are the same. For the wide range of positions and velocities encountered, the finite length analytical solution gives approximately the same results.

Figure 5 indicates the effect of doubling the unbalance eccentricity for both cases considered in Fig. 4. Note that the motion becomes one of circular synchronous precession with the finite length analytical solution having a slightly larger orbit. This is in agreement with other authors who

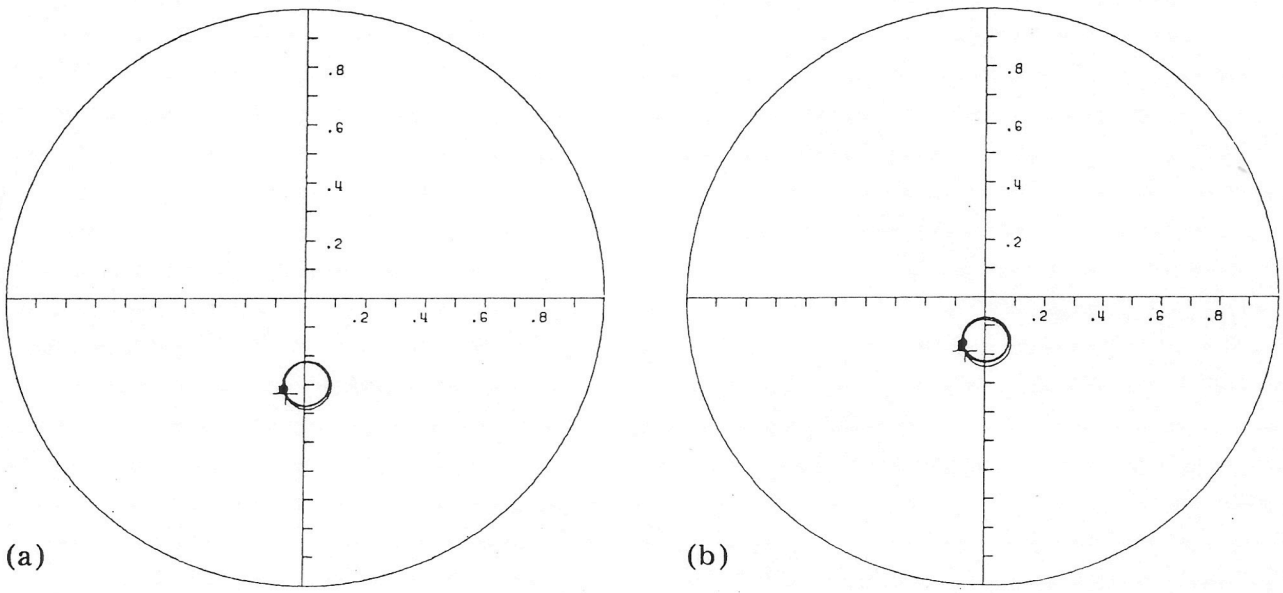


Fig. 6. Limit cycle of a damper with $L/D$ = 1.0 and $\bar{e}_u$ = 0.08. (a) Zero pre-load for a horizontal finite squeeze film bearing with a cavitated film. The parameters are as in Fig. 4(a) except: L 7.00 in; C 23.00 mil; TRD 0.44; FMAX 1621.4 lb. (b) 50% vertical pre-load for a horizontal finite squeeze film bearing with a cavitated film. The parameters are as in (a) except: TRD 0.37; FMAX 1381.4 lb; WY 337.50 lb.

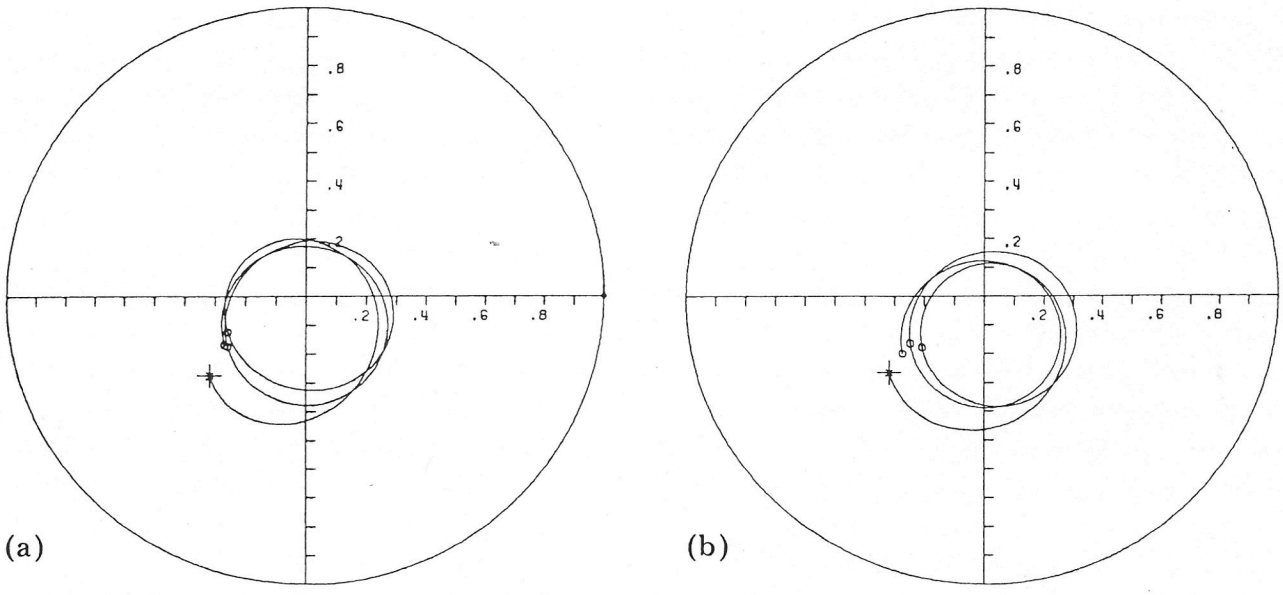


Fig. 7. Transient response of a damper with $L/D$ = 1.0, $\bar{e}_u$ = 0.25 and a zero vertical pre-load. (a) Short bearing approximation for a horizontal squeeze film bearing with a cavitated film. The parameters are as in Fig. 4(a) except: L 7.000 in; C 23.00 mil; FU 12 156.82 lb; TRD 0.56; FMAX 6826.4 lb. (b) Finite length theory for a horizontal finite squeeze film bearing with a cavitated film. The parameters are as in (a) except: TRD 0.34; FMAX 4098.1 lb.

The damper chosen using the theory in Section 3 is shown in Figs. 6 - 9 undergoing transient motions with various levels of vertical pre-load and unbalance. Vertical pre-loading of dampers tends to center the rotor relative to the damper housing. These results indicate that the initial damper design

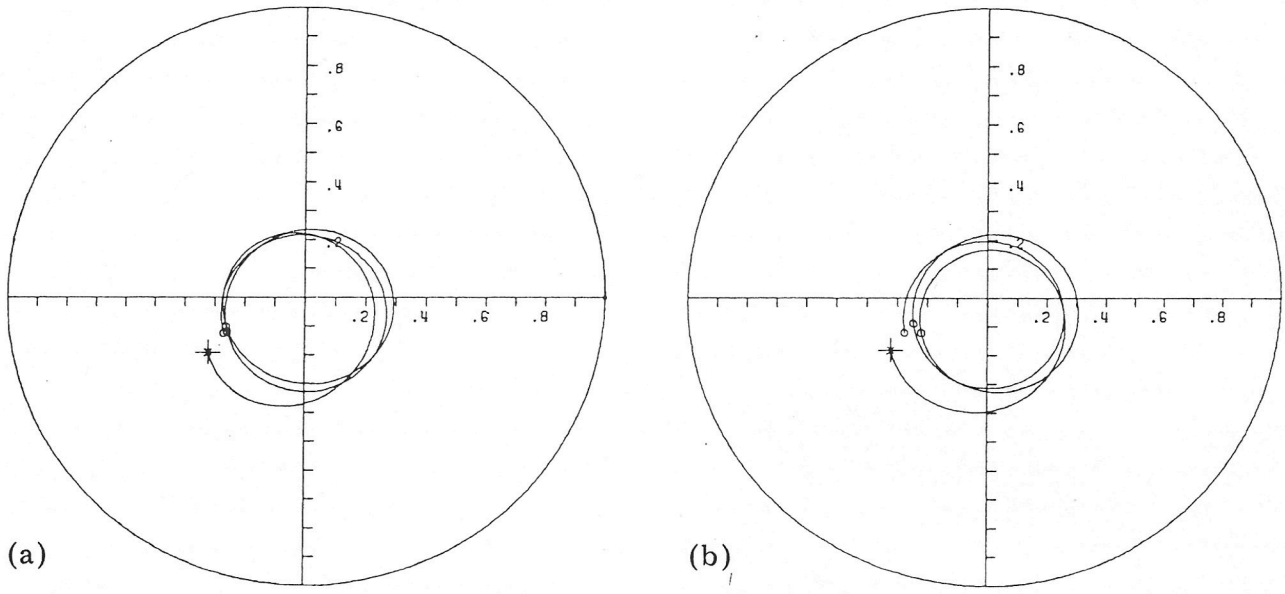


Fig. 8. Transient response of a damper with $L/D$ = 1.0, $e_u$ = 0.25 and a 50% vertical preload. (a) Short bearing approximation for a horizontal squeeze film bearing with a cavitated film. The parameters are as in Fig. 4(a) except: L 7.000 in; C 23.00 mil; FU 12 156.82 lb; TRD 0.46; FMAX 5604.1 lb; WY 337.50 lb. (b) Finite length theory for a horizontal finite squeeze film bearing with a cavitated film. The parameters are as in (a) except: TRD 0.30; FMAX 3618.0 lb.

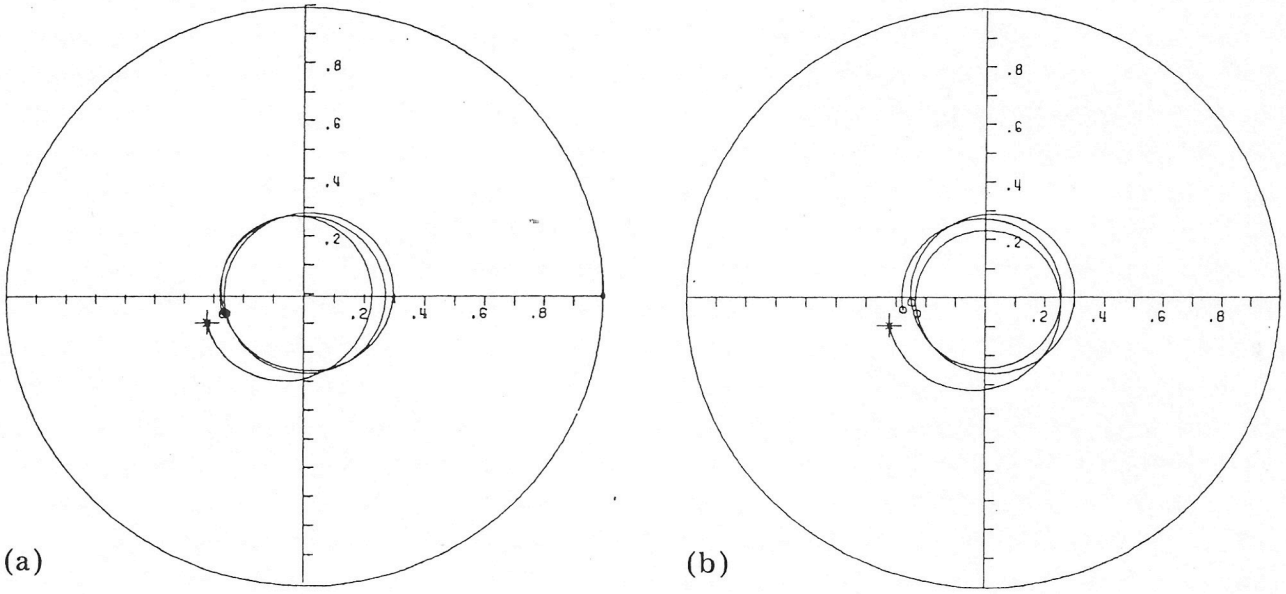


Fig. 9. Transient response of a damper with $L/D$ = 1.0, $e_u$ = 0.25 and a 100% vertical preload. (a) Short bearing approximation for a horizontal squeeze film bearing with a cavitated film. The parameters are as in Fig. 4(a) except: L 7.000 in; C 23.00 mil; FU 12 156.82 lb; TRD 0.34; FMAX 4073.2 lb. (b) Finite length theory for a horizontal finite squeeze film bearing with a cavitated film. The parameters are as in (a) except: TRD 0.21; FMAX 2599.2 lb.

Figure 6 shows that the orbit is circular and synchronous but that its center is not at the bearing center due to the small value of unbalance EMU = $\bar{e}$ = 0.08. This is comparable with the normal operating unbalance level. A 50%

to the support structure to the machinery FMAX from 7212 N (1621 lb) to 6144 N (1381 lb). Similarly the ratio TRD of the maximum force FMAX to the rotating unbalance force FU is reduced from 0.44 to 0.37. This is desirable, as values of TRD lower than one indicate lower forces transmitted with a damper than without.

A much higher level of unbalance EMU = 0.25 simulating blade loss or other significant change in unbalance is shown in Figs. 7 - 9. Figure 7(a) indicates the transient response carried out with short bearing theory while Fig. 7(b) gives the results using finite length theory. The two theories are in good agreement for $L/D = 2/7$, but for $L/D = 1.0$ the short bearing analysis gives results for FMAX 68% higher under identical starting conditions. Also Fig. 7(a) shows an orbit with center approximately at $\bar{y} = 0.10$ while Fig. 7(b) gives an orbit with center at $\bar{y} = 0.14$. Similar curves in Figs. 8 and 9 with a vertical pre-load yield a 55% and a 57% larger result, respectively, for the short bearing.

The effect of pre-loading the damper is beneficial. A 50% vertical pre-load, shown in Fig. 8(a), reduces TRD from 0.34 to 0.30 while a 100% pre-load, shown in Fig. 9(a), yields a value for TRD of 0.21.

## 5. Conclusions

(1) Variational analysis has been extended to general dynamic damper motion for finite length dampers. The pressure in the damper can be evaluated in terms of a doubly infinite trigonometric series which can be integrated analytically term by term to obtain the load capacity.

(2) Effective stiffness and damping coefficients for the damper have been obtained for circular synchronous precession about the damper center. As the $L/D$ ratio increases, the dimensionless coefficients decrease in magnitude for a given operating eccentricity.

(3) A comparison of short bearing theory and the finite length analytical solution shows good agreement for $L/D = 2/7$. The short bearing gives slightly larger load capacities in agreement with other authors.

(4) The use of short bearing theory for large $L/D$ ratios gives errors in the range of 50 - 70% in the dynamic forces compared with finite length theory.

(5) The results indicate that linearized analysis provides initial design parameters for dampers, but that the final design must be verified by nonlinear transient analysis.

(6) Vertical pre-loading of the rotor results in journal orbits which are more nearly centered in the damper housing and reduces the level of the transmitted forces. This may result in decreased rotor sensitivity to blade loss or other large unbalance excitation.

(7) Computer running time on a CDC 6400 system for the finite length analysis is approximately the same as that for the short bearing approach

## Nomenclature

| | |
|---|---|
| $A$, $B$ | Fourier series coefficients |
| $c$ | damper clearance |
| $C_0$, $\bar{C}_0$ | damping; $\bar{C}_0 = C_0(c/L)^3/\mu R$ |
| $D$ | diameter of journal |
| $e$, $\bar{e}$ | eccentricity; $\bar{e} = e/c$ |
| $e_u$, $\bar{e}_u$ | unbalance eccentricity; $\bar{e}_u = e_u/c$ |
| $F$, $\bar{F}$ | force; $\bar{F} = F/W$ |
| $h$, $\bar{h}$ | film thickness; $\bar{h} = h/c$ |
| $J$, $\bar{J}$ | functional; $\bar{J} = J/\rho c \omega W$ |
| $K_0$, $\bar{K}_0$ | stiffness; $\bar{K}_0 = K_0(c/L)^3/\mu R\omega$ |
| $L$, $\bar{L}$ | bearing length; $\bar{L} = L/D$ |
| $m$ | journal mass; $m = W/g$ |
| $N'$ | rotating speed in rev $s^{-1}$ |
| $P$, $\bar{P}$ | pressure; $\bar{P} = PDL/W$ |
| $S$ | Sommerfeld number: $\mu N' DL(R/c)^2/W$ |
| $t$, $\bar{t}$ | time; $\bar{t} = \omega t$ |
| $W$, $\bar{W}$ | journal weight; $\bar{W} = W/W = 1$ |
| $x$, $\bar{x}$ | horizontal displacement; $\bar{x} = x/c$ |
| $y$, $\bar{y}$ | vertical displacement; $\bar{y} = y/c$ |
| $z$, $\bar{z}$ | axial coordinate; $\bar{z} = z/L$ |
| $\alpha$ | $\theta - \theta_{max}$ |
| $\alpha_c$ | beginning of positive pressure region |
| $\theta$ | angular coordinate |
| $\theta_{max}$ | angle of maximum film thickness |
| $\mu$ | viscosity |
| $\omega$ | angular velocity |

## Acknowledgments

The work presented in this paper was sponsored in part by the U.S. Energy Research and Development Administration under contract no. E (49-18)-2479 F-01-76-0642 and in part by the U.S. Army Research Office.

## References

1 L. E. Barrett and E. J. Gunter, Steady state and transient analysis of a squeeze film damper bearing for rotor stability, NASA Contract. Rep. NASA-CR-2548, May, 1975.
2 M. D. Rabinowitz and E. J. Hahn, Squeeze Film Bearing Supports for Flexible Rotors, Inst. Mech. Eng., 1975, pp. 575 - 580.
3 R. E. Cunningham, D. P. Fleming and E. J. Gunter, Design of a squeeze film damper for a multi-mass flexible rotor, J. Eng. Ind., 97 (4) (1975) 1383 - 1389.
4 J. M. Vance and A. J. Kirton, Experimental measurement of the dynamic force response of a squeeze-film bearing damper, J. Eng. Ind., 97 (4) (1975) 1282 - 1290.
5 R. G. Kirk and E. J. Gunter, Stability and transient motion of a plain journal mounted in flexible damped supports, ASME Paper No. 75-DET-116, September, 1975.
6 J. Tonnesen, Experimental parametric study of a squeeze film bearing, ASME Paper No. 75-LUB-42, October, 1975.
7 E. J. Gunter, L. E. Barrett and P. E. Allaire, Design and application of squeeze film

8 D. F. Hays, Squeeze films: a finite journal bearing with a fluctuating load, J. Basic Eng., 83 (1961) 579 - 588.
9 D. F. Hays, A variational approach to lubrication problems and the solution of the finite journal bearing, J. Basic Eng., 81 (1959) 13 - 23.
10 F. W. Ocvirk, Short bearing approximation for full journal bearings, NACA Tech. Mem. NACA TN 2808, 1952.
11 R. G. Kirk and E. J. Gunter, Non-linear transient analysis of multi-mass flexible rotors — theory and applications, NASA Contract. Rep. NASA CR-2300, September, 1973.

## Appendix

The purpose of this appendix is to develop the algebraic equations for the coefficients $A_{kl}$ and $B_{kl}$ in the trigonometric pressure series. Equation (2) gives the film thickness as

$$\bar{h} = 1 + \bar{e} \cos (\theta - \theta_{max})$$

with

$$\bar{e} = (\bar{x}^2 + \bar{y}^2)^{1/2} \qquad \phi = \tan^{-1} (\bar{y}/\bar{x}) \qquad \theta_{max} = \phi + \pi$$

The required expressions are

$$\frac{\partial \bar{h}}{\partial \bar{t}} = \frac{\partial \bar{e}}{\partial \bar{t}} \cos \alpha + \bar{e} \frac{\partial \alpha}{\partial \bar{t}} \sin \alpha$$

$$\bar{h}^3 = c_0 + c_1 \cos \alpha + c_2 \cos 2\alpha + c_3 \cos 3\alpha$$

where

$$c_0 = 1 + \frac{3}{2} \bar{e}^2 \qquad c_1 = 3\bar{e} \left(1 + \frac{\bar{e}^2}{4}\right)$$

$$c_3 = \frac{3}{2} \bar{e}^2 \qquad c_4 = \frac{\bar{e}^3}{4}$$

Substitution of the series expression for $P$ (eqn. (8)) into eqn. (3) and applying the first part of eqn. (9) yields the equation for $A_{kl}$ as

$$2c_0 \{4k^2 + b^2\} A_{k,l} + c_1 \{4k(k+1) + b^2\} A_{k+1,l} +$$

$$+ c_1 \{4k(k-1) + b^2\} A_{k-1,l} + c_2 \{4k(k+2) + b^2\} (A_{k+2,l} - A_{2-k,l}) +$$

$$+ c_2 \{4k(k-2) + b^2\} A_{k-2,l} + c_3 \{4k(k+3) + b^2\} A_{k+3,l} +$$

$$+ c_3 \{4k(k-3) + b^2\} (A_{k-3,l} - A_{3-k,l})$$

$$= \begin{cases} -\dfrac{768\, S}{l} \dfrac{\partial \phi}{\partial \bar{t}} & \text{if } k = 1 \text{ and } l \text{ is odd} \end{cases}$$

where $b = \pi l/\bar{L}$. Similarly from the second part of eqn. (9) the equation for $B_{kl}$ is

$$
\begin{aligned}
&2c_0\{4(k-1)^2 + b^2\}(B_{k,l} + B_{2-k,l}) + c_1\{4k(k-1) + b^2\}B_{k+1,l} + \\
&+ c_1\{4(k-1)(k-2) + b^2\}(B_{k-1,l} + B_{3-k,l}) + \\
&+ c_2\{4(k-1)(k+1) + b^2\}B_{k+2,l} + c_2\{4(k-1)(k-3) + b^2\}(B_{k-2,l} + \\
&+ B_{4-k,l}) + c_3\{4(k-1)(k+2) + b^2\}B_{k+3,l} + \\
&+ c_3\{4(k-1)(k-4) + b^2\}(B_{k-3,l} + B_{5-k,l}) + c_1 k\langle 3-k\rangle b^2 B_{3-k,l} + \\
&+ 2c_2 b^2\{\langle 2-k\rangle + \langle k-2\rangle\langle 4-k\rangle\}B_{4-k,l} + \\
&+ 2c_3 b^2\{\langle 2-k\rangle + \langle k-3\rangle\langle 5-k\rangle\}B_{5-k,l}
\end{aligned}
$$

$$
= \begin{cases} -\dfrac{768\,S}{l}\dfrac{\partial \bar{e}}{\partial \bar{t}} & \text{if } k = 2 \text{ and } l \text{ is odd} \\ 0 & \text{otherwise} \end{cases} \qquad \text{(A2)}
$$

where the brackets $\langle\ \rangle$ denote a singularity function.

This result differs from previous results [8] in that the coefficients of both the sine and cosine are present. Hays' application considered only a 180° damper and purely vertical squeeze motions enabling the cosine terms to be dropped at the beginning of the analysis. Inclusion of the 360° damper with full non-linear dynamic effects results in the additional set of equations.

For the case of a 180° film, eqns. (10) and (11) become

$$
\begin{aligned}
\bar{F}_r = \frac{1}{\pi}\sum_{\substack{l=1\\ \text{odd}}}^{\infty}\frac{1}{l}\Bigg[ &-2B_{1,l}\sin\alpha_c + \frac{\pi}{2}B_{2,l} + \\
&+ \sum_{k=1}^{\infty}\Bigg\{ A_{2k,l}\,\frac{(2k-1)\cos(2k+1)\alpha_c + (2k+1)\cos(2k-1)\alpha_c}{4k^2-1} - \\
&- B_{2k+1,l}\,\frac{(2k+1)\sin(2k-1)\alpha_c + (2k-1)\sin(2k+1)\alpha_c}{4k^2-1}\Bigg\}\Bigg]
\end{aligned} \qquad \text{(A3)}
$$

$$
\begin{aligned}
\bar{F}_t = \frac{1}{\pi}\sum_{\substack{l=1\\ \text{odd}}}^{\infty}\frac{1}{l}\Bigg[ &\frac{\pi}{2}A_{1,l} + 2B_{1,l}\cos\alpha_c + \\
&+ \sum_{k=1}^{\infty}\Bigg\{ A_{2k,l}\,\frac{(2k-1)\sin(2k+1)\alpha_c - (2k+1)\sin(2k-1)\alpha_c}{4k^2-1} + \\
&+ B_{2k+1,l}\,\frac{(2k+1)\cos(2k-1)\alpha_c - (2k-1)\cos(2k+1)\alpha_c}{4k^2-1}\Bigg\}\Bigg]
\end{aligned}
$$

$$+ B_{2k+1,l} \frac{(2k-1)\cos(2k+1)\alpha_c - (2k+1)\cos(2k-1)\alpha_c}{4k^2-1} \Bigg\} \Bigg] \quad \text{(A4)}$$

This result applies to non-pressurized dampers of plain configuration with open ends or with end seals and circumferential supply grooves.